Advanced Topics in Lightwave Communications
Generation of Optical Signals

Keang-Po Ho

February 24, 2005

1 Direction-Modulation of Semiconductor Laser

In all optical communication systems, a light source must be used to originate an optical signal. Because of its small size, low power consumption, reliability, and compatible with electronic circuits, semiconductor diode lasers are the most widely used light source for communication applications. Virtually all optical communication systems use semiconductor laser as light source. Erbium-doped fiber amplifiers (EDFA) are also commonly pumped by high-power semiconductor lasers (Becker et al., 1999, Desurvire, 1994, Nakazawa et al., 1989). Other than lightwave communications, semiconductor laser also find its applications for optical data storage, like compact disk (CD) or digital versatile disk (DVD) machines.

1.1 Basic Structures

Figure 1 shows the basic structure of a semiconductor laser with a Fabry-Perot cavity. The active region is the media to provide optical gain sandwiched between the p- and n-type semiconductor materials. The p-n junction is preference to be a double-heterostructure junction in which the active region using a material having a band-gap smaller than both p- and n-type materials. The usage of heterostructure structure for semiconductor laser has two major advantages. Because of the band-gap difference, the active region can effectively confine electrons and holes into the active layer. Electron and hole recombination generates light or amplifies the passing through light through spontaneous and stimulated emission, respectively. The active region based on heterostructure also has larger refractive index. Similar to the principle of light guiding in an optical fiber, the active region acts as a dielectric slab waveguide to confine the light.

The laser cavity of the semiconductor laser of Fig. 1 is a Fabry-Perot resonator with two reflective mirrors at both sides. When light reaches one of the facets, part of the light reflects back to the active region as an optical feedback signal. In the most basic structure, the mirrors of semiconductor laser are

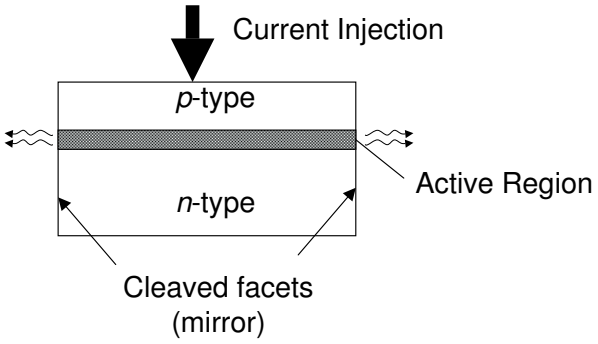

Figure 1: Structure of a semiconductor laser with a Fabry-Perot cavity.

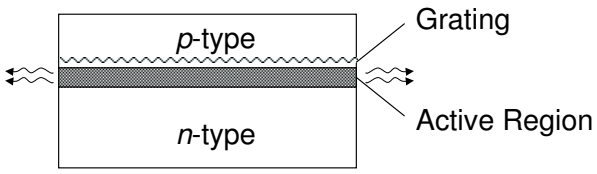

Figure 2: Structure of a distributed-feedback (DFB) semiconductor laser.

formed simply by cleaving with a reflectivity of

$$r_m = \left(\frac{n_r - 1}{n_r + 1}\right)^2, \tag{1}$$

where n_r is the refractive index of the gain medium. Typical for most semiconductor lasers, $n_r = 3.5$ and $r_m = 30\%$. For a semiconductor laser to generate light, the round-trip optical gain must be equal to the overall cavity loss. When current is injected into the p-n junction, the semiconductor laser reaches its lasing threshold when the optical gain is just equal to the cavity loss. In semiconductor laser, the optical gain is very large such that high facet loss can be tolerated.

For a cavity length of L_l, the modes of the Fabry-Perot cavity have a spacing of $c/(2n_rL_l)$, where c is the speed of light in free space. Note that the refractive index of n_r may change to n_{eff} to include the effect of the slab waveguide. For a typical length of $L_l = 200 - 400$ μm, the mode spacing of the laser is about 100 to 200 GHz, or about 1 to 2 nm at the wavelength around 1.55 μm.

The gain medium of semiconductor laser has a gain bandwidth on the order of 100 nm (about 12 THz). At least tens of modes can be supported within the gain bandwidth. In the semiconductor gain medium, due to heterogeneous broadening, the gain is reduced for the lasing wavelength with strong optical power. When the gain at the strong mode is reduced, the other modes can reach the same gain as the strong mode and start lasing. With tens of modes within the gain bandwidth, a semiconductor laser may have tens of lasing wavelengths. To limit the mode number in semiconductor laser, frequency selective loss can be introduced into the laser cavity. In additional to the Fabry-Perot resonator to limit the lasing wavelength to tones that are $c/2n_rL_l$ apart, frequency dependent structure can be introduced close to the active region of Fig. 1.

Figure 2 shows a distributed-feedback (DFB) laser with a grating close to the active region. The grating gives periodic variation of the waveguide refractive index. Instead of two facets, optical feedback is provided in the whole cavity in a DFB laser. The waves propagating in the forward and backward directions are coupled with each other. With the grating, coupling occurs only for wavelength λ_B with the Bragg condition of

$$\Lambda_g = m\frac{\lambda_B}{2n_{\text{eff}}}, \tag{2}$$

where Λ_g is the grating period, n_{eff} is the effective refractive index of the active region of the DFB laser, and m is the order of Bragg diffraction. The coupling between the forward and backward waves is the strongest for the first-order Bragg diffraction of $m = 1$. In order to operate a laser at $\lambda_B = 1.55$ μm, Λ_g is about 235 nm for $m = 1$ for $n_{\text{eff}} = 3.3$. Such grating can be fabricated by the interferometric pattern of two short wavelength laser beams or electron beam writing.

First operated in the liquid nitrogen temperature of 77 K° (Hall et al., 1962) and then the room temperature (Hayashi et al., 1970), various types of semiconductor laser are described in more details in the books of Agrawal and Dutta (1986), Casey and Panish (1978), and Coldren and Corzine (1995). The DFB structure was first proposed by Kogelnik and Shank (1971). In additional to the DFB structure, there is also a distributed Bragg reflection (DBR) structure with the grating at one end of the waveguide of Fig. 2 (Suematsu et al., 1983). As a variation of DFB laser, $\lambda/4$-shifted DFB laser has a $\lambda/4$ shift in the middle of the grating to provide a $\pi/2$ phase shift (Akiba et al., 1987). Other advanced semiconductor laser structures were reviewed in Suematsu et al. (1992), including the low-cost surface-emitting

semiconductor lasers (Iga et al., 1988). DFB laser for WDM applications was reviewed in Funabashi et al. (2004).

In additional to single wavelength DFB laser, there are also monolithically integrated widely tunable multiple wavelength semiconductor lasers (Coldren, 2000, Coldren et al., 2004), external cavity diode lasers tuned by micro-electro-mechanical systems (MEMS) (Anthon et al., 2002), or an array of DFB lasers selected by MEMS (Pezeshki et al., 2002). Those widely tunable lasers can cover the whole C- or L-band for EDFA.

The output intensity of a semiconductor laser follows its injected current. On-off keying signal may be generated by the presence or absence of injection current to turn-on and -off the semiconductor laser. Later in this section presents the rate equations to govern the laser dynamic.

Even when a semiconductor laser has a constant injection current, the output intensity of the semiconductor laser is noisy due to the spontaneous emission in the lasing material. External modulated system that uses a diode laser with constant injection current is still affected by the semiconductor laser noise. The laser phase noise directly affects a phase-modulated signal and laser intensity noise directly affects an on-off keying or amplitude-modulated signal. As a second-order effect, laser phase noise may convert to amplitude noise due to fiber chromatic dispersion.

1.2 Rate Equations and Laser Dynamic

The dynamic and noise characteristics of a semiconductor laser can be described by the laser rate equations. In its simplest way, a semiconductor laser converts electrons to photons. The laser electric field E_L and the carrier density n_c as a function of time are governed by the following rate equations

$$\frac{dE_L}{dt} = -j\Delta\omega(n_c)E_L + \frac{1}{2}\left[G(n_c) - \frac{1}{\tau_p}\right]E_L + F_n(t), \tag{3}$$

$$\frac{dn_c}{dt} = I_c - \frac{n_c}{\tau_c} - G(n_c)|E_L|^2, \tag{4}$$

where $\Delta\omega(n_c)$ is the deviation of oscillation angular frequency from the natural frequency of the laser cavity as a function of carrier density of n_c, $G(n_c)$ is the power gain as a function of carrier density n_c, τ_p is the lifetime of the photon particle, $F_n(t)$ is the Langevin random force caused by spontaneous emission, and I_c is the rate of carrier injection, and τ_c is the carrier lifetime. In the equation of Eq. (3), the electric field of E_L should have a unit such that the photon density in the laser cavity is $p_c = |E_L|^2$.

The physical meaning of the above rate equations is obvious. The first term of the right hand side of Eq. (3) is the frequency detuning due to carrier injection. In the stationary condition, $\Delta\omega(n_c) = 0$. The second term of the right hand side of Eq. (3) is the gain of electric field provided by the lasing medium. Because the laser light losses due to material absorption, emitted out from the laser cavity, the electric field (or photon) has a photon lifetime of τ_p depending on the laser cavity. If the overall loss of the cavity is r_c due to mirror and internal material loss, the photon lifetime is equal to $\tau_p^{-1} = v_g r_c$ where v_g is the group velocity of light. The last term of the right hand side of Eq. (3) is due to spontaneous emission. The Langevin force of $F_n(t)$ is usually modeled as a complex value white Gaussian noise. The carrier rate equation of Eq. (4) also has simple physical meaning. I_c is the rate of carrier increase due to current injection, τ_c is the carrier lifetime, and the last term of Eq. (4) is the carrier converting to photons. For a current density of I_d, the rate of carrier injection is $I_c = I_d/e$, where e is the electron charge The detuning of $\Delta\omega(n_c)$ just affects the phase of the electric field E_L and thus the term of $-j\Delta\omega(n_c)E_L$ with the multiplication of "j".

The refractive index of semiconductor material is equal to $n_r(n_c) = n_0 + \Delta n_r(n_c) + j\Delta n_i(n_c)$, where n_0 is the refractive index without carrier injection, $n_r(n_c)$ and $n_i(n_c)$ are the real and imaginary parts of the refractive index as a function of carrier density n_c. The gain of $G(n_c)$ is proportional to the imaginary refractive index of $-\Delta n_i(n_c)$. The lasing frequency should be aligned with the mode spacing of $n_r(n_c)/L_l c$. The term of $\Delta n_r(n_c)$ induces fluctuation in resonance frequency of the cavity and gives $\Delta\omega(n_c)$, generating frequency modulation by carrier injection.

When the semiconductor laser is biased well above the lasing threshold with a small signal injection current of

$$I_c = I_{c0} + \Re\{v_m e^{j\omega_m t}\}, \tag{5}$$

where v_m and ω_m are the modulation amplitude and frequency, respectively. The electric field and the carrier density have stationary values of $E_0 = \sqrt{P_{c0}}e^{j\phi_0}$ and N_0. The rate equations of Eqs. (3) and (4) can be linearized around E_0 and N_0 for $E_L(t) = \sqrt{P_{c0} + \Delta p(t)}e^{j\phi_0 + j\phi_n(t)}$ and $n_c(t) = N_0 + \Delta n(t)$. First of all, both frequency detuning $\Delta\omega(n_c)$ and medium gain $G(n_c)$ are linearized by

$$\Delta\omega(n_c) = -\frac{\partial\omega}{\partial n_c}\Delta n, \tag{6}$$

$$G(n_c) = G(N_0) + \frac{\partial G}{\partial n_c}\Delta n. \tag{7}$$

Ignores the Langevin noise of F_n, the rate equations become

$$\frac{d\phi_n}{dt} = \frac{\partial\omega}{\partial n_c}\Delta n, \tag{8}$$

$$\frac{d\Delta p}{dt} = P_{c0}\frac{\partial G}{\partial n_c}\Delta n, \tag{9}$$

$$\frac{d\Delta n}{dt} = \Delta i_c - \left(\frac{1}{\tau_c} + P_{c0}\frac{\partial G}{\partial n_c}\right)\Delta n - G(N_0)\Delta p, \tag{10}$$

where $\Delta i_c = \Re\{v_m e^{j\omega_m t}\}$. The photon density is

$$\Delta p(\omega_m) = \frac{P_{c0}\frac{\partial G}{\partial n_c}v_m}{\omega_R^2 - \omega_m^2 + j\gamma_e\omega_m}, \tag{11}$$

where

$$\omega_R^2 = P_{c0}G(N_0)\frac{\partial G}{\partial n_c}, \tag{12}$$

$$\gamma_e = \frac{1}{\tau_c} + P_{c0}\frac{\partial G}{\partial n_c} \tag{13}$$

as the resonance frequency and damping rate of relaxation oscillation. In semiconductor laser, the differential gain of $\partial G/\partial n_c$ is almost a constant above lasing threshold. The relaxation frequency of ω_R of Eq. (12) increases with both the photon density of P_{c0} and the gain of the laser $G(N_0)$. In general, ω_R increases almost linearly with P_{c0}.

The normalized modulation response of a semiconductor laser is the transfer function of

$$H_p(\omega_m) = \frac{\Delta p(\omega_m)}{\Delta p(0)} = \frac{\omega_R^2}{\omega_R^2 - \omega_m^2 + j\gamma_e\omega_m}. \tag{14}$$

The instantaneous frequency of a laser is $\frac{1}{2\pi}d\phi_n(t)/dt$. The response of the laser frequency can be written as

$$\dot{\phi}_n(\omega_m) = \frac{j\omega}{2P_{c0}}\frac{\frac{\partial\omega}{\partial n_c}}{\frac{1}{2}\frac{\partial G}{\partial n_c}}\Delta p(\omega_m). \tag{15}$$

The factor of

$$\alpha = \frac{\frac{\partial\omega_m}{\partial n_c}}{\frac{1}{2}\frac{\partial G}{\partial n_c}} \tag{16}$$

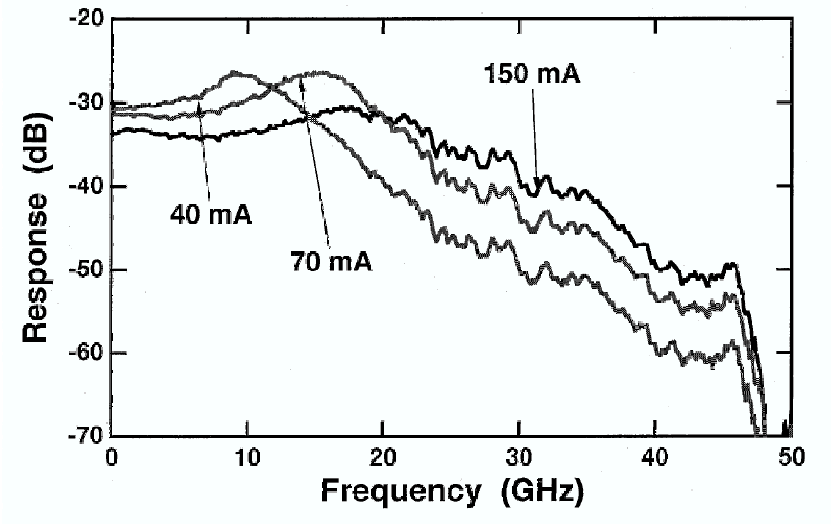

Figure 3: The measured small-signal amplitude response of a high-speed semiconductor laser. [From Sato (2002), © 2005 IEEE]

is the linewidth enhancement factor. The linewidth enhancement factor of α can also be rewritten as

$$\alpha = \frac{\dfrac{\partial n_r}{\partial n_c}}{\dfrac{\partial n_i}{\partial n_c}}, \tag{17}$$

where n_r and n_i represent the real and imaginary parts of the effective refractive index. The linewidth enhancement factor of commonly used DFB laser is about 3 to 4.

The response of the laser phase is

$$\dot{\phi}_n(\omega_m) = \frac{\alpha}{2P_{c0}} j\omega_m \Delta p(\omega_m). \tag{18}$$

The normalized transfer function of the laser frequency is

$$H_{\dot{\phi}}(\omega_m) = \frac{j\omega_m \omega_R^2}{\omega_R^2 - \omega_m^2 + j\gamma_e \omega_m}. \tag{19}$$

The transfer function of Eq. (19) will be revisited later in this chapter about direct frequency modulation of a semiconductor laser.

Figure 3 shows the photon response of direct-modulation of a high-speed semiconductor laser used for 40-Gb/s applications (Sato, 2002, Sato et al., 2002). The laser response has a second-order response of Eq. (14). Similar to Eq. (12), the relaxation oscillation frequency increases with the bias current or the output power.

The method to analyze laser dynamic here follows the books of Petermann (1991) and Okoshi and Kikuchi (1988). Laser dynamic can also be studied based on the rate equations of the carrier density and photon density (Lau and Yariv, 1985, Tucker, 1985, Tucker and Kaminow, 1984). Further increase of current injection generates more photons, but the optical gain is reduced to $G(n_c)(1 - \epsilon_{\rm NL} p_c)$, where $\epsilon_{\rm NL}$ is a nonlinear-gain parameter due to saturation effect. In semiconductor material, due to heterogeneous broadening, the factor of $\epsilon_{\rm NL}$ depends on wavelength. Nonlinear gain saturation is a major factor that affect the laser dynamic (Lau and Yariv, 1985, Olshansky et al., 1987, Ralston et al., 1993, Tucker, 1985). The relaxation peaks of the amplitude response of Fig. 3 is reduced due to the contribution of $\epsilon_{\rm NL}$ (Ralston et al., 1993) or laser parasitic (Tucker and Kaminow, 1984). High-speed semiconductor laser with a speed of 20 to 40 GHz has been developed (Kjebon et al., 1997, Matsui et al., 1997, Morton

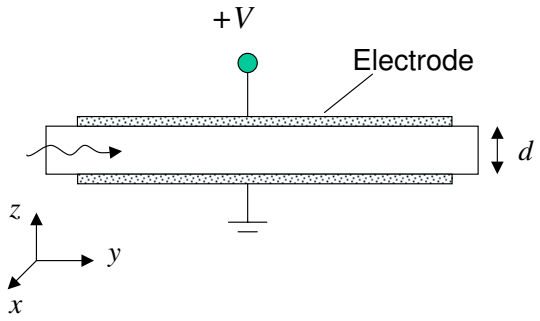

Figure 4: Structure to illustrate the operation of a phase modulator.

et al., 1992, Ralston et al., 1993, Weisser et al., 1996). Semiconductor laser can be directly modulated for 40-Gb/s data rate (Sato, 2002, Sato et al., 2002). The parameters for the rate equations of Eqs. (3) and (4) can be found using parameter extraction methods (Cartledge and Srinivasan, 1997, Lee et al., 2002, Salgado et al., 1997).

2 External Modulators

External modulators provide the best signal quality for both phase and amplitude modulated signals. An electro-optical crystal with proper orientation provides phase modulation with a voltage applied in the right direction. Lithium Niobate ($LiNbO_3$) is the most commonly used electro-optical crystal to fabricate external modulator. In this section, external modulator using $LiNbO_3$ is assumed by default.

2.1 Phase Modulator

The generation of a phase-modulated signal requires an external modulator capable of changing the optical phase in response to an applied voltage. In $LiNbO_3$, if an electric field is applied along the z-axis of the crystal, the refractive index of the material is changed by

$$\Delta n = \frac{1}{2} n_r^3 r_{33} E_z, \tag{20}$$

where r_{33} is the electro-optic coefficient for a change of refractive index n_r for light propagating along the z-direction, and E_z is the electric field along the z direction. When a voltage is applied to the electro-optical material, the electric field of E_z is approximately equal to V/d, where d is the distance between the two electrodes. The total phase shift over an interaction length of L_i is

$$\Delta\phi_0 = \frac{2\pi \Delta n L_i}{\lambda_c} = \pi n_r^3 r_{33} \frac{V L_i}{d\lambda}, \tag{21}$$

where λ is the wavelength of the optical signal.

The voltage necessary to provide a phase shift of 180° is equal to

$$V_\pi = \frac{d\lambda}{n_r^3 r_{33} L_i}. \tag{22}$$

In the design of a phase modulator, one of the main purpose is to reduce the voltage of V_π. The electro-optic coefficient of r_{33} in $LiNbO_3$ is the largest among all coefficients for various orientations (Turner, 1966). The parameter of $n_r^3 r_{33}$ of $LiNbO_3$ is equal to $328 \times 10^{-6} \mu$m/V(Alferness, 1982).

In the bulk modulator structure of Fig. 4, the modulator V_π can be reduced by increasing the interaction length of L_i or reducing the electrode distance of d. However, the capacitance of the capacitor formed between the two electrodes is proportional to L_i/d. The reduction of V_π increases the capacitance and slows down the operation of the modulator.

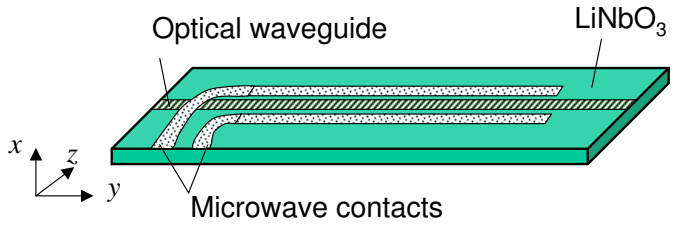

Figure 5: Illustration of a waveguide based traveling-wave phase modulator.

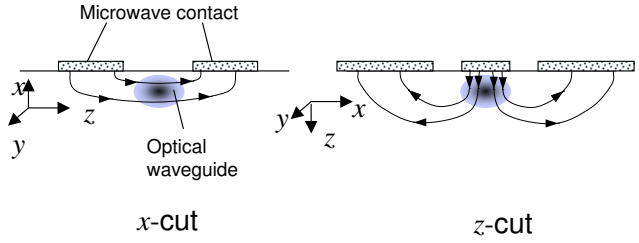

Figure 6: Waveguide based traveling-wave phase modulator using x- or z-cut $LiNbO_3$ materials.

Figure 5 shows a traveling-wave phase modulator. In principle, if the light in the optical waveguide and modulated electrical signal in the microwave electrodes are traveling in the same speed, the traveling-wave phase modulator of Fig. 5 has infinite bandwidth. $LiNbO_3$ has a refractive index of about $n_r = 2.1$ to 2.2. The microwave signal must slow down to close to the speed of c/n_r of the optical signal. The design of the microwave waveguide must match to the traveling speed of optical signal in $LiNbO_3$ for high-speed operation.

In the waveguide phase modulator of Fig. 5, there are two methods to couple electric field into the optical waveguide. Figure 6 shows two waveguide structures using either x- or z-cut $LiNbO_3$ crystal. The electric field lines are along the z-axis in both cases. Using the x-cut material, the electrodes for the transmission line are located in either side of the optical waveguide. Using the z-cut material, the electrode for applied drive signal is located exactly on the top of the optical waveguide. Usually, the z-cut phase modulator has better coupling efficiency between the electric field and the optical waveguide. The V_π of the modulator is still the same as that of Eq. (22) with the distance of d taking into account the overlapping between electric and optical fields, i.e., an effective separation of d instead of the physical separation.

2.1.1 Effects of Velocity Mismatch

If the microwave electrode impedance is matched to the connecting cable and signal source, the microwave drive signal along the transmission line is

$$V(z,t) = V_0 \Re\left\{e^{j\beta_m z - j\omega_m t}\right\}, \tag{23}$$

where ω_m is the angular frequency of the microwave signal, and $\beta_m = \omega_m n_m/c + j\alpha_m$ is the propagation constant of the microwave signal with n_m as the effective refractive index of the microwave waveguide, z is the distance from the beginning of the microwave and optical waveguide, and α_m is the loss coefficient of the microwave signal. Traveling with a speed of c/n_r, the photon entering the optical waveguide at any time t_0 experiences a voltage of

$$\begin{aligned} V(z,t_0) &= V_0 \Re\left\{\exp\left[j\beta_m z - j\omega_m\left(t_0 + \frac{zn_r}{c}\right)\right]\right\} \\ &= V_0 e^{-\alpha_m z}\Re\left\{e^{j\omega_m d_{12} z - j\omega_m t_0}\right\} \end{aligned} \tag{24}$$

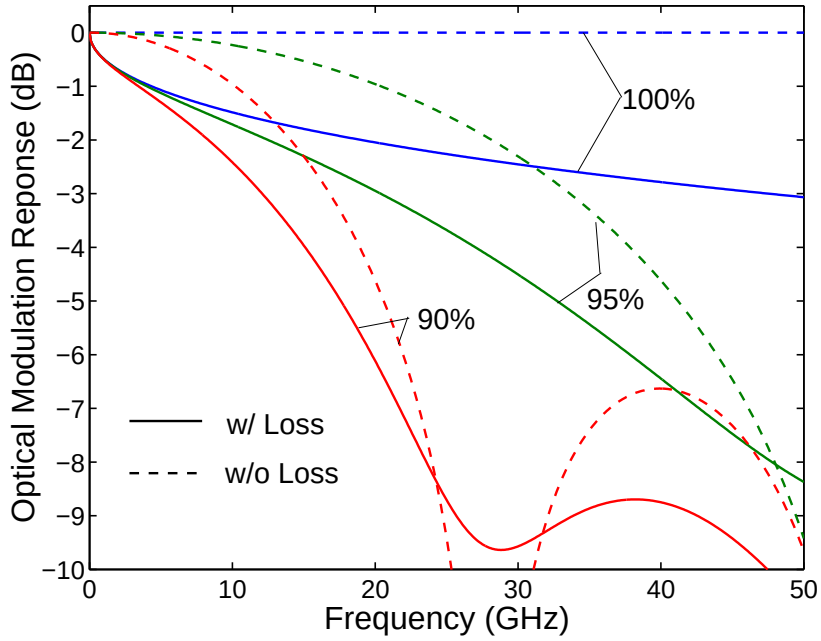

Figure 7: Effects of velocity mismatch of a phase modulation.

at a distance of z from the input of the waveguide, where $d_{12} = (n_m - n_r)/c$ is the walk-off parameter between microwave and optical fields. For a waveguide length of L, the overall phase shift is

$$\Delta\phi(\omega_m) = \frac{\Delta\phi_0}{L_i} \frac{1 - e^{-\alpha_m L + j d_{12}\omega_m L}}{\alpha_m - j d_{12}\omega_m} \tag{25}$$

as a function of the modulation frequency of ω_m, where $\Delta\phi_0$ is the phase shift from Eq. (21) and $L_i = (1 - e^{-\alpha_m L})/\alpha_m$ is the effective interaction length. For a d.c. voltage with $\omega_m = 0$, the phase shift is $\Delta\phi(0) = \Delta\phi_0$. Without waveguide loss of $\alpha_m = 0$, the frequency response is proportional to the sinc function of $\sin(x)/x$ with $x = d_{12}\omega_m L/2$.

Figure 7 shows the frequency response of a phase modulator with velocity mismatch. The microwave loss is assumed to be either without loss of $\alpha_m = 0$ or $\alpha_m = \alpha_{m0}\sqrt{f_m}$ due to skin effect, where $f_m = \omega_m/2\pi$ is the modulation frequency. The loss coefficient is $\alpha_{m0} = 0.2$ dB/cm/$\sqrt{\text{GHz}}$ (Kondo et al., 2002, Sugiyama et al., 2002). The length of the modulator is assumed to be $L = 5$ cm (Sugiyama et al., 2002). With microwave loss, Figure 7 shows that the velocity matching of only 95% reduces the bandwidth from 50 GHz to less than 22 GHz. In the design of external modulator, in additional to impedance match and loss reduction, the design of the electrode for velocity matching is an important issue (Gopalakrishnan et al., 1994, Kawano et al., 1991, Koshiba et al., 1999).

2.2 Amplitude Modulator

An amplitude-shift keying (ASK) signal can be generated using an amplitude or intensity modulator to turn-on and -off the light. Amplitude modulator functions as a very fast switch. While semiconductor laser can be directly modulated, direct modulation of a semiconductor laser comes with frequency chirp. An external amplitude modulator usually provides very a high quality signal.

Figure 8 shows an amplitude modulator based on the simple equal path-length Mach-Zehnder interferometer. The input optical signal is splitted into two paths via a **Y** junction. For illustration purpose, one of the optical path is phase-modulated and another path remains unmodulated. If the **Y** junction splits the input signal of E_i into two equal electric fields of $E_i/\sqrt{2}$ each, ignored the path delay, some constant phase shifts, and waveguide loss, the combined signal at another end of the **Y** junction is

$$E_o = \frac{E_i}{2}\left[1 + \exp\left(j\pi\frac{V(t)}{V_\pi}\right)\right]$$

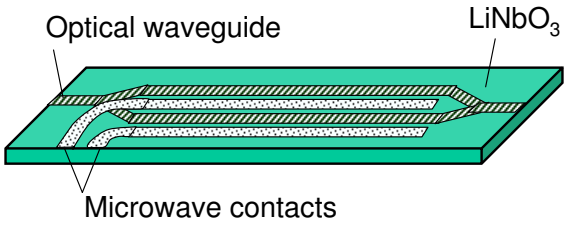

Figure 8: Basic schematic of an amplitude modulator based on Mach-Zehnder interferometer.

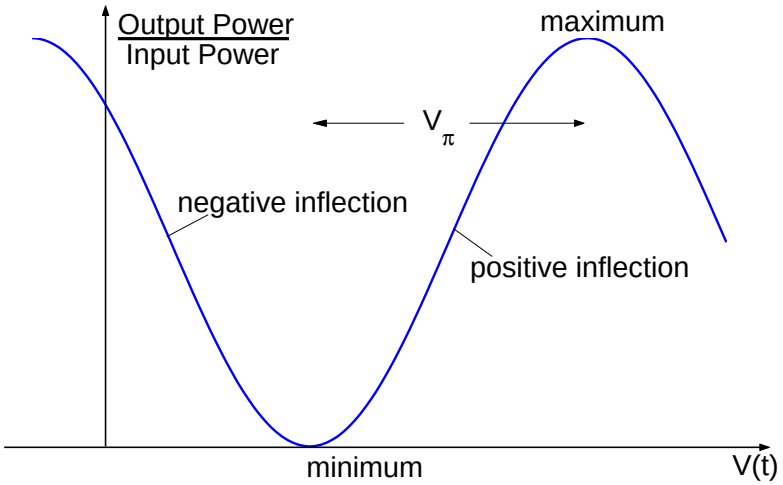

Figure 9: Input-output transfer characteristic of a Mach-Zehnder modulator.

$$= E_i \cos\left[\frac{\pi}{2}\frac{V(t)}{V_\pi}\right] \exp\left[j\frac{\pi}{2}\frac{V(t)}{V_\pi}\right], \tag{26}$$

where V_π is the parameter of the phase modulator at the lower path of Fig. 8. From Eq. (26), in term of optical intensity, the input and output relationship of a Mach-Zehnder intensity modulation is

$$\frac{|E_o|^2}{|E_i|^2} = \cos^2\left[\frac{\pi}{2}\frac{V(t)}{V_\pi}\right], \tag{27}$$

as a nonlinear sinusoidal transfer function shown in Fig. 9. The voltage to turn the modulator from minimum to maximum transmission points is V_π. Because of some amount of constant phase shift, $V(t) = 0$ in practical modulator is not necessary corresponding to the maximum transmission point as shown in Figure 9.

However, in additional to the change of optical intensity, the input and output relationship of Eq. (26) also accompanies with phase modulation of $\exp[j\phi(t)]$ with $\phi(t) = \pi V(t)/2V_\pi$. The ratio of phase to amplitude modulation is called chirp parameter (Koyama and Oga, 1988). The Mach-Zehnder modulator in the schematic of Fig. 8 has a chirp parameter of ± 1 with the plus or minus sign depending on whether the amplitude modulator is operated in the positive or negative inflection points of Fig. 9, respectively. In additional to chirp, the unmodulated path of Fig. 8 reduces the modulation efficiency of the modulator. When the microwave electrodes are properly designed, both paths of the Mach-Zehnder modulator can be modulated to improve the modulator efficiency.

Figure 10 shows three different waveguide structures for a Mach-Zehnder modulator using x- and z-cut $LiNbO_3$ crystal. Using the x-cut crystal, the two paths of the Mach-Zehnder modulator are phase-modulated with opposite phase shifts in a push-pull structure. For the input-output relationship of Fig. 9, the V_π is reduced by half with respect to the single electrode schematic of Fig. 8. Because the two paths are modulated with opposite phases of $\pm\pi V(t)/2V_\pi$ with a parameter of V_π representing the

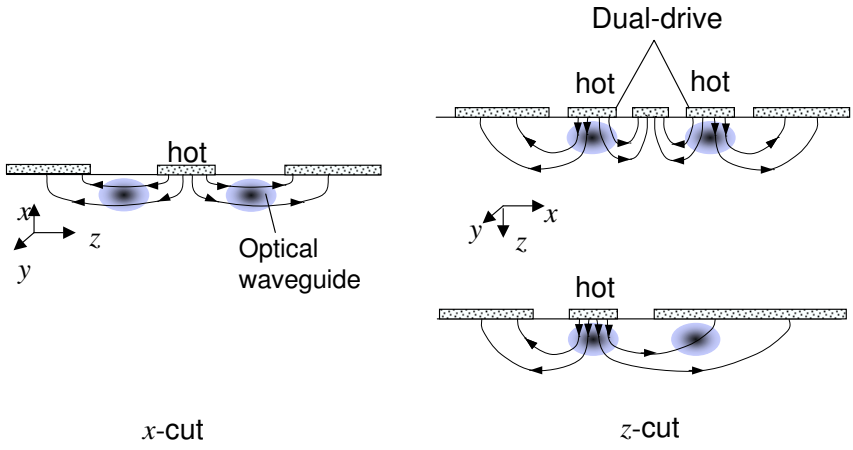

Figure 10: Three different structures for Mach-Zehnder modulator using x- or z-cut $LiNbO_3$.

combined V_π of the two phase modulators, the output field corresponding to Eq. (26) is

$$\begin{aligned} E_o &= \frac{E_i}{2}\left[\exp\left(-j\pi\frac{V(t)}{2V_\pi}\right)+\exp\left(j\pi\frac{V(t)}{2V_\pi}\right)\right] \\ &= E_i\cos\left[\frac{\pi}{2}\frac{V(t)}{V_\pi}\right]. \end{aligned} \tag{28}$$

In the single-drive x-cut push-pull modulator of Fig. 10, no phase modulation accompanies the amplitude modulation from Eq. (28) and the modulator has zero-chirp. In term of optical intensity, the transfer characteristic follows Eq. (27) or Fig. 9. The input and output transfer characteristic of Eq. (28) may also provide 0 and π phase modulation to an optical single. For $V(t)$ from 0 to V_π, E_o and E_i have the same phase. For $V(t)$ from V_π to $2V_\pi$, E_o and E_i has opposite phases. Phase modulation provided by zero-chirp modulator has the advantage that amplitude jitter does not give phase jitter, i.e., variation of drive voltage does not transfer to variation of output phase. However, the phase modulation is limited to 0 and π, equivalent to ± 1. For phase-modulation operation to minimize loss and obtain optimal amplitude jitter compression, the modulator should operate between two maximum transmission points for a peak-to-peak voltage swing of $2V_\pi$.

Figure 10 shows two waveguide configurations using z-cut $LiNbO_3$ crystal. Assume that the two paths have identical structure, the chirp coefficient is equal to (Koyama and Oga, 1988)

$$\alpha = \frac{V_1(t)+V_2(t)}{V_1(t)-V_2(t)}, \tag{29}$$

where $V_1(t)$ and $V_2(t)$ is the drive voltage of the two paths, respectively. When the two paths are driven by complementary signal with $V_1(t) = -V_2(t)$, the modulated signal has zero-chirp. In the dual-drive structure, the modulator chirp is adjustable (Gnauck et al., 1991).

The single-drive configuration of Fig. 10 for z-cut modulator usually has nonzero chirp coefficient because the electric field lines pass through the two optical waveguides are usually not the same. In normal operation, the chirp coefficient for single-drive z-cut modulator is about ± 0.75 (Schiess and Carlden, 1994). With proper waveguide arrangement, the single drive z-cut modulator can be designed as zero-chirp modulator with reduced efficiency. If the dual-drive z-cut modulator is operated as a single-drive modulator with one hot electrode connected to ground, the chirp coefficient is also about the same as a single-drive z-cut modulator of about ± 0.75.

In on-off keying for IMDD system, the modulator chirp can be used to compensate for fiber dispersion (Gnauck et al., 1991). In ASK for coherent optical communications, additional phase modulation is not desirable and should be reduced. Currently, most commercially available amplitude modulator is $LiNbO_3$ Mach-Zehnder modulator of Fig. 10 (Wooten et al., 2000). Earlier amplitude modulator has

various structures besides the Mach-Zehnder interferometer (Alferness, 1981, 1982, 1990, Korotky and Alferness, 1988, Kubota et al., 1980). Instead of just a phase modulator like Fig. 5 (Kawano et al., 1989, Tench et al., 1987), after 90's, high-speed modulators are designed mostly for amplitude modulation (Burns et al., 1999, Dolfi et al., 1988, Fujiwara et al., 1990, Howerton et al., 2000, Noguchi et al., 1998, 1995, Wooten et al., 2000). Currently, dual-drive 40 Gb/s modulator with a V_π of less than 2 V has been demonstrated experimentally (Sugiyama et al., 2002). Even experimental x-cut modulator has a V_π less than 3 V (Aoki et al., 2004, Kondo et al., 2002). Commercially available $LiNbO_3$ amplitude modulator has a V_π from 4 to 6 V. In additional to $LiNbO_3$, semiconductor materials also have electro-optical effect and can be used to fabricate external modulator (Alferness, 1981, Cites and Ashley, 1994, Leonberger and Donnelly, 1990, Tsuzuki et al., 2004, Walker, 1987, 1991, Yu et al., 1996). Even silicon has electro-optical effect that can be used for modulator (Dainesi et al., 2000, Jackson et al., 1998, Liu et al., 2004). External modulator can also use the electro-optical effect in polymer (Chen et al., 1997, Dalton et al., 1999, Lee et al., 2000, Oh et al., 2001, Shi et al., 1996, 2000). With a refractive index smaller than that of $LiNbO_3$, the speed of electrical and optical signals may be matched in polymer modulator without major engineering efforts. The electro-optic coefficient of other materials are listed in Liu (1996), Saleh and Teich (1991), and Yariv (1997).

The **Y** junction of the Mach-Zehnder modulator of Fig. 8 should split the optical signal into two equal parts. If the power splitting ratio is not equal to unity but a factor of, for example, γ_s, the ratio of the power at the maximum to the minimum transmission point of Fig. 9 is equal to

$$r_{\text{ex}} = \left(\frac{1+\gamma_s}{1-\gamma_s}\right)^2. \tag{30}$$

The ratio of r_{ex} is the extinction ratio. Most commercially available $LiNbO_3$ Mach-Zehnder modulator has an extinction ratio larger than 20 dB at d.c. However, the extinction ratio for the eye-diagram is usually limited to 10 to 12 dB because of waveform ripples of the drive signal. Finite d.c. extinction ratio also induces chirp to the optical signal (Kim and Gnauck, 2002, Walklin and Conradi, 1997).

Semiconductor materials can be used to make electroabsorption modulator (EAM) based on Frank-Keldysh effect for bulk semiconductor and quantum-confined Stark effect for quantum well (Bennett and Soref, 1987, Miller et al., 1986, Wood, 1988). Together with amplitude moduation, electroabsorption modulator always gives a chirped output because of the accompany frequency modulation. Electroabsorption modulator can be integrated with many other components (Akulova et al., 2002, Frateschi et al., 2004, Johansson et al., 2004, Mason et al., 2002) or operated in very high-speed (Akage et al., 2001, Choi et al., 2002, Kawanishi et al., 2001, Miyazaki et al., 2003).

2.3 Operation of Amplitude Modulator

When a Mach-Zehnder modulator is biased at the middle positive inflection point and the drive signal has a peak-to-peak voltage of V_π, the baseband representation of the electric field at the output of the modulator is

$$\begin{aligned} E_o(t) &= \frac{E_i}{2}\left\{\exp\left[\frac{j(1+\alpha)\pi}{2}\frac{V(t)}{V_\pi}\right]\right. \\ &\qquad \left. +j\exp\left[-\frac{j(1-\alpha)\pi}{2}\frac{V(t)}{V_\pi}\right]\right\}, \end{aligned} \tag{31}$$

where α is the chirp coefficient, and $V(t)$ is the binary drive signal of

$$V(t) = \sum_{k=-\infty}^{+\infty} \frac{b_k V_\pi}{2} p(t-kT), \tag{32}$$

where $b_k = \pm 1$ is the transmitted random data stream, $p(t)$ is the pulse shape of the drive signal, and T is the bit interval of the data. The two terms in Eq. (31) correspond to the two phase-modulated

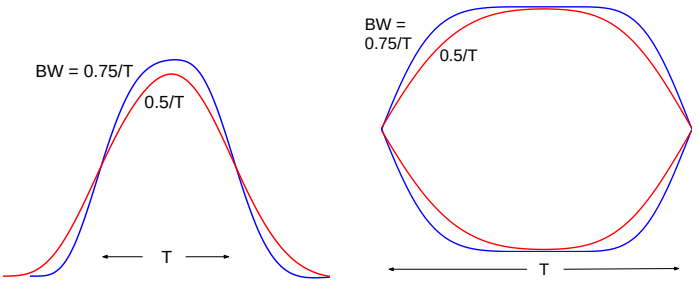

(a) $p(t)$ (b) $|E_o(t)|^2$

Figure 11: (a) Bessel-filtered pulse shape and (b) the corresponding eye-diagram of the optical intensity.

paths of the Mach-Zehnder modulator. The differential phase shift between the two phase modulators is $\pi V(t)/V_\pi$. The intensity of the modulator output of

$$|E_o(t)|^2 = |E_i(t)|^2 \sin\left[\frac{\pi}{4} + \frac{\pi}{2}\frac{V(t)}{V_\pi}\right]^2 \tag{33}$$

is independent of the chirp coefficient. When $V(t) = -V_\pi/2$, the output of $|E_o(t)| = 0$ locates at the minimum transmission point. When $V(t) = +V_\pi/2$, the output of $|E_o(t)| = |E_i(t)|^2$ is at the maximum transmission point. An external modulator is normally biased at the negative inflection point to give negative chirp for dispersion compensation(Gnauck et al., 1991). The bias at positive inflection point is used here for illustration propose.

The relation of Eq. (31) can be used to model all types of Mach-Zehnder modulators having different values of chirp coefficient α. For example, a dual-drive modulator has adjustable chirp, a single-drive z-cut modulator has a chirp coefficient of $\alpha = \pm 0.75$, and an x-cut push-pull Mach-Zehnder modulator has zero chirp. Because most external modulators have very large extinction ratio, the expression Eq. (31) assumes an infinite extinction ratio.

Ideally, the Mach-Zehnder modulator should be driven by a rectangular pulse that has been filtered by a Bessel lowpass filter. Figures 11 show both the pulse shape and the corresponding eye diagram when a fifth-order Bessel filter having a bandwidth of either $0.75/T$ or $0.5/T$ is used[1], where T is the bit interval for the binary signal. Owing to the nonlinear transfer characteristic of the Mach-Zehnder modulator, a bandwidth of $0.5/T$ is sufficient to provide an good eye-diagram in optical intensity, but then the receiver must have a very wide bandwidth to preserve the eye opening to the decision circuits.

While the eye-diagram of Fig. 11(b) does not change with the chirp coefficient, the phase of the output electric field of $E_o(t)$ of Eq. (31) varies with chirp coefficient. Figure 12 shows the electric field locus changing from the off-state of $(0, 0)$ to the on-state at the unit circle shown as dash-line. The intersection point corresponds to the bias point of $V(t) = 0$ located at $(1/2, 1/2)$. Using a zero-chirp modulator with $\alpha = 0$, the electric field has a constant angle of $\pi/4$. However, with a chirp modulator, the phase changes with the instantaneous drive voltage. With a chirp coefficient of $\alpha = \pm 1$, the output electric field changes along a circle ending at $(0, 1)$ and $(1, 0)$, respectively. The locus of Fig. 12 depends only on the chirp coefficient but independent to the waveform of the drive signal.

Figures 13 show the single-sided optical spectrum of the optical signal modulated by a random pulse stream with a Bessel-filtered pulse given by Fig. 11(a). Fifth-order Bessel filters have bandwidths of $0.75/T$ and $0.5/T$ for Figs. 13(a) and (b), respectively. Figs. 13 also show the optical spectra for different values of the chirp coefficient of $\alpha = 0, \pm 0.5, \pm 1$. For comparison, Figs. 13 also plot the electrical spectrum of the drive signal $V(t)$ for comparison.

[1]The fifth-order Bessel filter has a response of

$$H(s) = \frac{945}{945 + 945s + 420s^2 + 105s^3 + 15s^4 + s^5}$$

where $s = jf/f_0$ with f_0 adjust for different bandwidth.

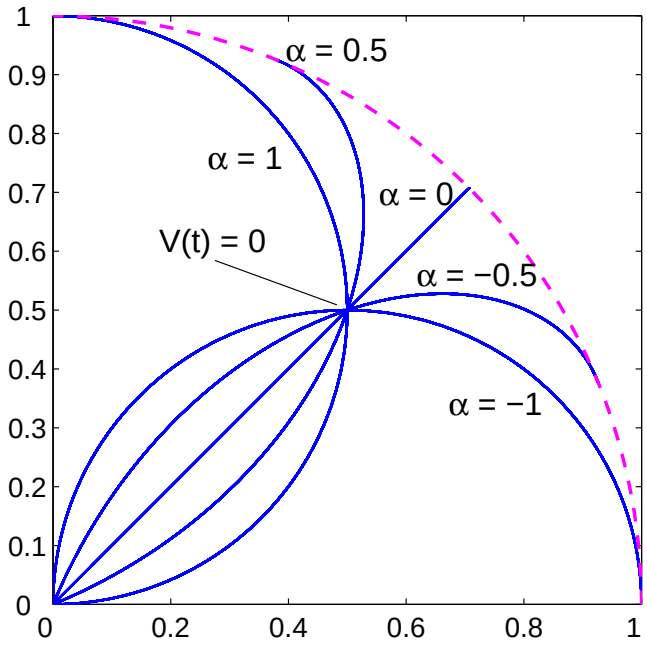

Figure 12: The phase change from turn-on to -off of an amplitude modulator biased at the positive middle inflection point. The dashed circle is the on state and the origin is the off state. The middle intersection corresponds the bias of $V(t) = 0$.

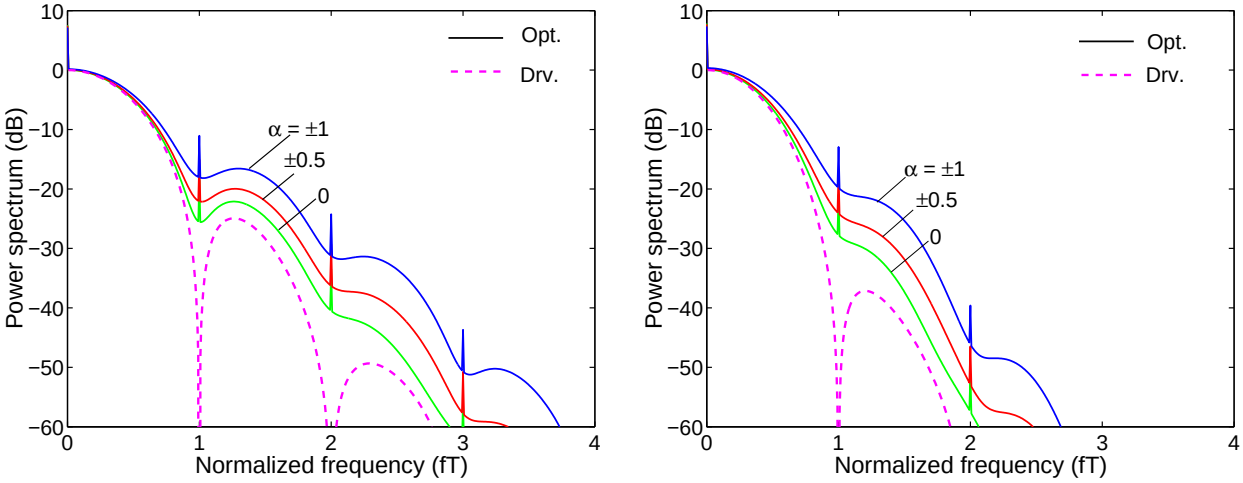

(a) BW $= 0.75/T$ (b) BW $= 0.5/T$

Figure 13: The power spectral density of an on-off keying optical signal when a Bessel-filtered pulse is used as the drive signal. The Bessel filter has a bandwidth of (a) $0.75/T$ and (b) $0.5/T$. The dashed lines are the electrical spectrum of the drive signal. [Adapted from Ho (2004)]

Modulator chirp broadens the optical spectrum of the signal. Figures 13 show that the approximation of the optical spectrum using the electrical spectrum of the drive signal underestimates the spectral spreading. The differences between the power spectra of $E_o(t)$ and $V(t)$ are more significant when the low-pass filter having the small bandwidth of $0.5/T$ is used. Figures 13 show that chirp broadens the optical spectrum, causing more broadening when a Bessel filter having smaller bandwidth, corresponding to longer rise and fall times, is used.

In Figs. 13, there are major differences at the integer normalized frequencies of $fT = \pm 1, \pm 2, \ldots$. While the electrical spectrum of the drive signal of $V(t)$ has notches at those normalized frequencies, the optical spectrum has discrete tones at those same frequencies, and also has a tone at $f = 0$ due to the d.c. value of the electric field. The differences between the power spectra of $E_o(t)$ and that of $V(t)$ are more significant when the Bessel filtered pulse has smaller bandwidth. When the pulse bandwidth is $0.75/T$, the difference is about 3 dB at the second lobe of $fT = 1.5$ for $\alpha = 0$. When the pulse bandwidth is $0.5/T$, the second lobe is at about $fT = 1.25$, the difference increases to about 5 to 12 dB even for a chirp coefficient of $\alpha = 0$.

The effect of the chirp coefficient also depends on the pulse bandwidth. With a bandwidth of $0.75/T$, the chirp coefficient does not change the optical power spectral density as much as when the bandwidth is $0.5/T$. By comparing Figs. 13(a) and (b), we may also conclude that the modulator chirp has a greater effect for a drive signal having longer rise or fall times.

The operation of amplitude modulator is well-known in most optical communication textbooks (Agrawal, 2002, Keiser, 1999, Liu, 1996). The power spectrum of chirp modulated signal was first analyzed by Ho and Kahn (2004) using the method of Greenstein (1977), Ho (1999), and Ho et al. (2000). Of course, the optical spectrum is routinely measured or simulated for phase-modulated or IMDD optical communication systems.

For the long-term operation of an amplitude modulator based on $LiNbO_3$, the bias voltage must be actively controlled to compensate for the d.c. drift (Korotky and Veselka, 1996, Nagata, 2000, Nagata et al., 2004). Low-speed controller is usually used for bias control to maintain the optimal biasing point for the modulator.

2.4 Generation of RZ-DPSK Signals

Among all digital modulation formats for phase-modulated optical communications, DPSK signal may be the most popular scheme using the phase difference of optical carrier to carry information. DPSK signals typically use return-to-zero (RZ) linecode.

Figure 14 is a transmitter to generate RZ-DPSK signal using the cascade of an amplitude and phase modulator. The amplitude or intensity modulator is preference to have zero-chirp and generate an RZ pulse train. The phase modulator modulates the phase of the RZ pulse train to generate the RZ-DPSK signal. The drive signal of the phase modulator should be preceded by a precoder to calculate the cumulative parity of the input sequence. In Fig. 14, the phases of all pulses given by the amplitude modulator are assumed to be identical or alternating.

The pulse generator of Fig. 14 is an amplitude modulator driven by a sinusoidal signal synchronized with the data source. The drive signal of the phase modulator must be arrived to the modulator at the same time as the pulse for optimal performance.

Figure 15 shows three different methods to generate the pulse train for RZ-DPSK transmitter of Fig. 14. Figure 15(a) is the sinusoidal drive signal. Figures 15(b) and (c) are the output pulse train in optical intensity when the amplitude modulator is biased at the maximum and minimum transmission point of Fig. 9, respectively. From Figs. 15(b) and (c), when biased at either minimum or maximum transmission points, the pulse rate is twice the frequency of the sinusoidal drive signal of Fig. 15(a). In additional to pulse train generation, the frequency doubling property had also been used for electro-optical mixer (Ho et al., 1997, Sun et al., 1996).

The sinusoidal drive signal of Fig. 15(a) has a peak-to-peak voltage of $2V_\pi$ for the output pulse trains of Figs. 15(b) and (c). The duty cycles of the pulse train of Figs. 15(b) and (c) are 1/3 and 2/3, respectively. The pulse train of Fig. 15(b) biased at the maximum transmission point has the same optical phase at

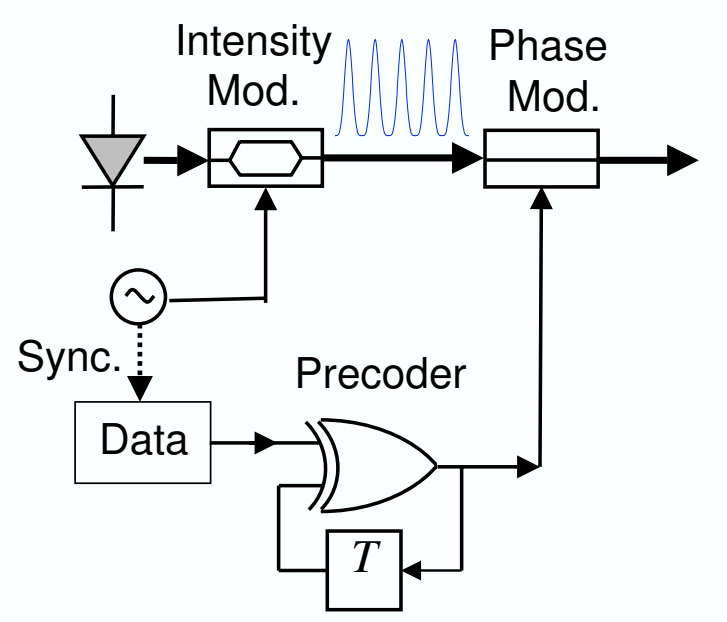

Figure 14: Schematic of transmitter to generate RZ-DPSK signals.

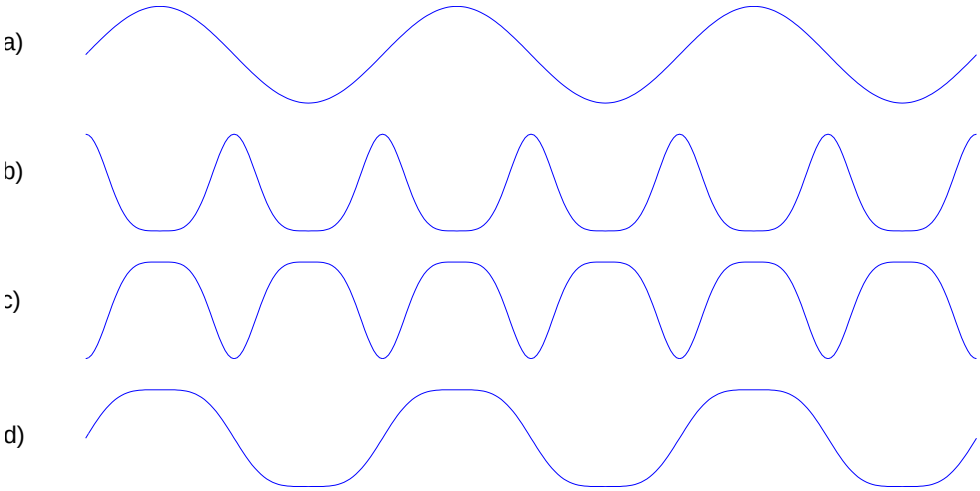

Figure 15: Pulse generation for RZ-DPSK modulation: (a) is the driving signal, (b), (c), and (c) are the output intensity. The output pulse trains of (b) and (c) use a driving swing of $2V_\pi$ and bias at maximum and minimum transmission points, respectively. The output pulse trains of (d) use a driving swing of V_π and biases at either the positive or negative inflection point.

all pulses. However, the pulse train of Fig. 15(c) biased at the minimum transmission point has the opposite optical phase of 0 and π at adjacent pulses. The pulse train of Fig. 15(c) is commonly called carrier-suppressed RZ (CSRZ) pulse. Even with opposite phases at adjacent pulses, the precoder of Fig. 14 is still the same but operated with an inverted transmitted data, or the received signal can be inverted after the decision circuits.

The pulse train of Fig. 15(d) is generated by the sinusoidal drive signal of Fig. 15(a) with V_π of peak-to-peak voltage swing. The amplitude modulator is based at either the positive or negative inflection point. The rate of the pulse train of Fig. 15(d) is the same as the frequency of the sinusoidal drive signal of Fig. 15(a). The phase of all pulses in the pulse train of Fig. 15(d) is identical. The duty cycle of the pulse train is 1/2.

To obtain DPSK signal, the phase modulator in Fig. 14 may be a simple phase modulator or a zero-chirp amplitude modulator. From the transfer function of Eq. (28) for zero-chirp modulator, amplitude modulator can provide phase modulation. In steady state, if $V(t) = \{0, 2V_\pi\}$, the output electric field is $E_0 = \pm E_i$ with a phase difference of 180°. Note that amplitude ripples deviated from 0 and $2V_\pi$ do not give a phase other than 0 and 180°. The nonlinear transfer characteristic of Eq. (27) also gives intensity compression to the output signal. The amplitude ripples are compressed in the output intensity.

In additional to the dual-modulator configuration of Fig. 15 to generate RZ-DPSK signal, a single-drive zero-chirp modulator can be used to generate NRZ-DPSK signal. The drive signal is a NRZ signal with a peak-to-peak voltage swing of $2V_\pi$. The modulator must be biased at the minimum transmission point. The drive voltage swings between two maximum transmission points of the transfer characteristic of Fig. 9 with phase difference of 180°. The operation of the modulator with and without the phase difference of 180° generates NRZ-DPSK signal. Normally, the modulator is operated with a bias at V_π with a signal swing between $\pm V_\pi$.

The transmitter of RZ-DPSK signal similar to Fig. 14 was first used by Gnauck et al. (2002) and explained in more detail in both Xu et al. (2004) and Gnauck and Winzer (2005). The locations of RZ and DPSK modulators of Fig. 14 can be interchanged without changing the function of the transmitter. Wen et al. (2004) proposed method to generate RZ-DPSK signal using only a single dual-drive modulator.

3 Summary

This chapter briefly introduces methods to generate an optical signal with modulation in amplitude, phase, or frequency to carry digital information. Semiconductor lasers are widely used as the light source for typical lightwave communication systems that also enable directly either amplitude or frequency modulation.

To provide better signal quality, external modulator is used to apply amplitude or phase modulation to an optical signal. External modulator based on electro-optical effect is also discussed in this chapter. Amplitude modulator is mostly used for on-off keying signal to block or unblock an optical signal. Amplitude modulator is also able to generate either PSK or DPSK signals for a phase difference of either 0 or π.

The popular RZ-DPSK signals are generated by the cascade of a RZ and phase modulators. The RZ duty cycle is typically 1/3, 1/2, and 2/3.

References

Agrawal, G. P. (2002). *Fiber-Optic Communication Systems*. Wiley-Interscience, New York, 3 edition.

Agrawal, G. P. and Dutta, N. K. (1986). *Long-Wavelength Semiconductor Lasers*. Van Norstrand-Reinhold, Princeton, NJ.

Akage, Y., Kawano, K., Oku, S., Iga, R., Okamoto, H., Miyamoto, Y., and Takeuchi, H. (2001). Wide bandwidth of over 50 GHz traveling-wave electrode electroabsorption modulator integrated DFB lasers. *Electron. Lett.*, 37(5):299–300.

Akiba, S., Usami, M., and Utaka, K. (1987). 1.5 μm $\lambda/4$-shifted InGaAsP/InP DFB lasers. *J. Lightwave Technol.*, LT-5(11):1564–1573.

Akulova, Y. A., Fish, G. A., Koh, P.-C., Schow, C. L., Kozodoy, P., Dahl, A. P., Nakagawa, S., Larson, M. C., Mack, M. P., Strand, T. A., Coldren, C. W., Hegblom, E., Penniman, S. K., Wipiejewski, T., and Coldren, L. A. (2002). Widely

tunable electroabsorption-modulated sampled-grating DBR laser transmitter. *IEEE J. Sel. Top. Quantum Electron.*, 8(6):1349–1357.

Alferness, R. C. (1981). Guided-wave devices for optical communication. *IEEE J. Quantum Electron.*, QE-17(6):946–959.

Alferness, R. C. (1982). Waveguide electrooptic modulators. *IEEE Trans. Microwave Theory & Tech.*, MTT-30(8):1121–1137. Erratum: MTT-31, no. 3, p. 315.

Alferness, R. C. (1990). Titanium-diffused Lithium Niobate waveguide devices. In Tamir, T., editor, *Guided-Wave Optoelectronics*, pages 145–210. Springer-Verlag, Berlin, 2 edition.

Anthon, D., Berger, J. D., Drake, J., Dutta, S., Fennema, A., Grade, J. D., Hrinya, S., Ilkov, F., Jerman, H., King, D., Lee, H., and Tselikov, A.and Yasumura, K. (2002). External cavity diode lasers tuned with silicon MEMS. In *Optical Fiber Commun. Conf.*, Optical Society of America, Washington, D.C. paper TuO7.

Aoki, K., Kondo, J., Kondo, A., Mori, T., Mizuno, Y., Shimodaira, S., Imaeda, M., Kozuka, Y., Mitomi, O., and Minakata, M. (2004). High-performance optical modulator with a wide center electrode and thin x-cut $LiNbO_3$ substrate. *IEEE Photon. Technol. Lett.*, 16(12):2610–2612.

Becker, P. C., Olsson, N. A., and Simpson, J. R. (1999). *Erbium-Doped Fiber Amplifiers: Fundamental and Technology.* Academic Press, San Diego.

Bennett, B. R. and Soref, R. A. (1987). Electrorefraction and electroabsorption in InP, GaAs, GaSb, InAs, and InSb. *IEEE J. Quantum Electron.*, QE-23(12):2159–2166.

Burns, W. K., Howerton, M. M., Moeller, R. P., R. Krähenbühl, R., McElhanon, R. W., and Greenblatt, A. S. (1999). Low drive voltage, broad-band $LiNbO_3$ modulators with and without etched ridges. *J. Lightwave Technol.*, 17(12):2551–2555.

Cartledge, J. C. and Srinivasan, R. C. (1997). Extraction of DFB laser rate equation parameters for system simulation purposes. *J. Lightwave Technol.*, 15(5):852–860.

Casey, H. C. and Panish, M. B. (1978). *Heterostructure Lasers.* Academic Press, San Diego.

Chen, D., Fetterman, H. R., Chen, A., Steier, W. H., Dalton, L. R., Wang, W., and Shi, Y. (1997). Demonstration of 110 GHz electro-optic polymer modulators. *Appl. Phys. Lett.*, 70(25):3335–3337.

Choi, W. J., Bond, A. E., Kim, J., Zhang, J., Jambunathan, R., Foulk, H., O'Brien, S., van Norman, J., Vandegrift, D., Wanamaker, C., Shakespeare, J., and Cao, H. (2002). Low insertion loss and low dispersion penalty InGaAsP quantum-well high-speed electroabsorption modulator for 40-Gb/s very-short-reach, long-reach, and long-haul applications. *J. Lightwave Technol.*, 20(12):2052–2056.

Cites, J. S. and Ashley, P. R. (1994). High-performance Mach-Zehnder modulators in multiple quantum well GaAs/AlGaAs. *J. Lightwave Technol.*, 12(7):1167–1173.

Coldren, L. A. (2000). Monolithic tunable diode lasers. *IEEE J. Sel. Top. Quantum Electron.*, 6(6):988–999.

Coldren, L. A. and Corzine, C. W. (1995). *Diode Lasers and Photonic Integrated Circuits.* John Wiley & Sons, New York.

Coldren, L. A., Fish, G. A., Akulova, Y., Barton, J. S., Johansson, L., and Coldren, C. W. (2004). Tunable semiconductor lasers: A tutorial. *J. Lightwave Technol.*, 22(1):193–202.

Dainesi, P., Küng, A., Chabloz, M., Lagos, A., Flückiger, P., Ionescu, A., Fazan, P., Declerq, M., Renaud, P., and Robert, P. (2000). CMOS compatible fully integrated Mach-Zehnder interferometer in SOI technology. *IEEE Photon. Technol. Lett.*, 12(6):660–662.

Dalton, L., Harper, A., Ren, A., Wang, F., Todorova, G., Zhang, J. C. C., and Lee, M. (1999). Polymeric electro-optic modulators: From chromophore design to integration with semiconductor very large scale integration electronics and silica fiber optics. *Ind. Eng. Chem. Res.*, 38(1):8–33.

Desurvire, E. (1994). *Erbium-Doped Fiber Amplifiers.* John Wiley & Sons, New York.

Dolfi, D. W., Nazarathy, M., and Jungerman, R. L. (1988). 40 GHz electro-optic modulator with 7.5 V drive voltage. *Electron. Lett.*, 24(9):528–529.

Frateschi, N. C., Zhang, J., Choi, W. J., Gebretsadik, H., Jambunathan, R., and Bond, A. E. (2004). High performance uncooled C-band, 10 Gbit/s InGaAlAs MQW electroabsorption modulator integrated to semiconductor amplifier in laser-integrated modules. *Electron. Lett.*, 40(2):140–141.

Fujiwara, T., Watanabe, A., and Mori, H. (1990). Measurement of uniformity of driving voltage in $Ti:LiNbO_3$ waveguides using Mach-Zehnder interferometers. *IEEE Photon. Technol. Lett.*, 2(4):260–261.

Funabashi, M., Nasu, H., Mukaihara, T., Kimoto, T., Shinagawa, T., Kise, T., Takaki, K., Takagi, T., Oike, M., Nomura, T., and Kasukawa, A. (2004). Recent advances in DFB lasers for ultradense WDM applications. *IEEE J. Sel. Top. Quantum Electron.*, 10(2):312–320.

Gnauck, A. H., Korotky, S. K., Veselka, J. J., Nagel, J., Kemmerer, C. T., Minford, W. J., and Moser, D. T. (1991). Dispersion penalty reduction using an optical modulator with adjustable chirp. *IEEE Photon. Technol. Lett.*, 3(10):916–918.

Gnauck, A. H., Raybon, G., Chandrasekhar, S., Leuthold, J., Doerr, C., Stulz, L., Agrawal, A., Banerjee, S., Grosz, D., Hunsche, S., Kung, A., Marhelyuk, A., Maymar, D., Movassaghi, M., Liu, X., Xu, C., Wei, X., and Gill, D. M. (2002). 2.5 Tb/s (64 × 42.7 Gb/s) transmission over 40 × 100 km NZDSF using RZ-DPSK format and all-Raman-amplified spans. In *Optical Fiber Commun. Conf.* Optical Society of America, Washington, D.C. postdeadline paper FC2.

Gnauck, A. H. and Winzer, P. J. (2005). Optical phase-shift-keyed transmission. *J. Lightwave Technol.*, 23(1):115–130.

Gopalakrishnan, G. K., Burns, W. K., McElhanon, R. W., Bulmer, C. H., and Greenblatt, A. S. (1994). Performance and

modeling of broadband $LiNbO_3$ traveling wave optical intensity modulators. *J. Lightwave Technol.*, 12(10):1807–1819.

Greenstein, L. J. (1977). Spectra of PSK signals with overlapping baseband pulses. *IEEE Trans. Commun.*, COM-25(5):523–530.

Hall, A. N., Fenner, G. E., Kingsley, T. D., Soltyo, T. I., and Carlson, R. O. (1962). Stimulated emission of radiation from GaAs *p-n* junctions. *Phys. Rev. Lett.*, 9(11):366–378.

Hayashi, I., Panish, M. B., Foy, P. W., and Sumelay, S. (1970). Junction lasers which operate continuously at room temperature. *Appl. Phys. Lett.*, 17(3):109–111.

Ho, K.-P. (1999). Spectral density of cross-phase modulation induced phase noise. *Opt. Commun.*, 169(1-6):63–68.

Ho, K.-P. (2004). Phase statistics of the soliton. *J. Opt. Soc. Amer. B*, 21(2):266–272.

Ho, K.-P. and Kahn, J. M. (2004). Spectrum of externally modulated optical signals. *J. Lightwave Technol.*, 22(2):658–663.

Ho, K.-P., Liaw, S.-K., and Lin, C. (1997). Efficient photonic mixer with frequency doubling. *IEEE Photon. Technol. Lett.*, 9(4):511–513.

Ho, K.-P., Yu, H., Chen, L.-K., and Tong, F. (2000). High-resolution measurement and spectral overlap of cross-phase modulation induced spectral broadening. *IEEE Photon. Technol. Lett.*, 12(11):1534–1536.

Howerton, M. M., Moeller, R. P., Greenblatt, A. S., and Krähenbühl, R. (2000). Fully packaged, broad-band $LiNbO_3$ modulator with low drive voltage. *IEEE Photon. Technol. Lett.*, 12(7):792–794.

Iga, K., Koyama, F., and Kinoshita, S. (1988). Surface emitting semiconductor lasers. *IEEE J. Quantum Electron.*, 24(9):1845–1855.

Jackson, S. M., Hewitt, P. D., Reed, G. T., Tang, C. K., Evans, A. G. R., Clark, J., Aveyard, C., and Namavar, F. (1998). A novel optical phase modulator design suitable for phased arrays. *J. Lightwave Technol.*, 16(11):2016–2019.

Johansson, L. A., Akulova, Y. A., Fish, G. A., and Coldren, L. A. (2004). Sampled-grating DBR laser integrated with SOA and tandem electroabsorption modulator for chirp-control. *Electron. Lett.*, 40(1):70–71.

Kawanishi, H., Yamauchi, Y., Mineo, N., Shibuya, Y., Mural, H., Yamada, K., and Wada, H. (2001). EAM-integrated DFB laser modules with more than 40-GHz bandwidth. *IEEE Photon. Technol. Lett.*, 13(9):954–956.

Kawano, K., Kitoh, T., Mitomi, O., Nozawa, T., and Jumonji, H. (1989). A wide-band and low-driving-power phase modulator employing a Ti:$LiNbO_3$ optical waveguide at 1.5 μm. *IEEE Photon. Technol. Lett.*, 1(2):33–34.

Kawano, K., Noguchi, K., Kitoh, T., and Miyazawa, H. (1991). A finite element method (FEM) analysis of a shielded velocity-matched Ti:$LiNbO_3$ optical modulator. *IEEE Photon. Technol. Lett.*, 3(10):919–921.

Keiser, G. (1999). *Optical Fiber Communications*. McGraw Hill, New York, 3 edition.

Kim, H. and Gnauck, A. H. (2002). Chirp characteristics of dual-drive, Mach-Zehnder modulator with a finite DC extinction ratio. *IEEE Photon. Technol. Lett.*, 12(3):298–300.

Kjebon, O., Schatz, R., Lourdudoss, S., Nilsson, N., Stålnacke, B., and Bäckborn, L. (1997). 30 GHz direct modulation bandwidth in detuned loaded InGaAsP DBR lasers at 1.55 μm wavelength. *Electron. Lett.*, 33(6):488–489.

Kogelnik, H. and Shank, C. V. (1971). Stimulated emission in a periodic structure. *Appl. Phys. Lett.*, 18(4):152–154.

Kondo, J., Kondo, A., Aoki, K., Takatsuji, S., Mitomi, O., Imaeda, M., Kozuka, Y., and Minakata, M. (2002). 40-Gb/s *x*-cut $LiNbO_3$ optical modulator with two-step back-slot structure. *J. Lightwave Technol.*, 20(12):2110–2114.

Korotky, S. K. and Alferness, R. C. (1988). Waveguide electrooptic devices for optical communication. In Miller, S. E. and Kaminow, I. P., editors, *Optic Fiber Telecommunications II*, chapter 11, pages 421–465. Academic Press, San Diego.

Korotky, S. K. and Veselka, J. J. (1996). An RC network analysis of long term Ti:$LiNbO_3$ bias stability. *J. Lightwave Technol.*, 14(12):2687–2697.

Koshiba, M., Tsuji, Y., and Nishio, M. (1999). Finite-element modeling of broad-band traveling-wave optical modulators. *IEEE Trans. Microwave Theory & Tech.*, 47(9):1627–1633.

Koyama, F. and Oga, K. (1988). Frequency chirping in external modulators. *J. Lightwave Technol.*, 6(1):87–93.

Kubota, K., Noda, J., and Mikami, O. (1980). Traveling wave optical modulator using a directional coupler $LiNbO_3$ waveguide. *IEEE J. Quantum Electron.*, QE-16(7):754–760.

Lau, K. Y. and Yariv, A. (1985). Ultra-high speed semiconductor lasers. *IEEE J. Quantum Electron.*, QE-21(2):121–138.

Lee, J., Nam, S., Lee, S. H., and Jeong, J. (2002). A complete small-signal equivalent circuit model of cooled butterfly-type 2.5 Gbps DFB laser modules and its application to improve high frequency characteristics. *IEEE Trans. Adv. Packaging*, 25(4):543–548.

Lee, S. S., Garner, S. M., Chuyanov, V., Zhang, H., Steier, W. H., Wang, F., Dalton, L. R., Udupa, A. H., and Fetterman, H. R. (2000). Optical intensity modulator based on a novel electrooptic polymer incorporating a high $\mu\beta$ chromophore. *IEEE J. Quantum Electron.*, 36(5):527–532.

Leonberger, F. J. and Donnelly, J. P. (1990). Semiconductor integrated optic devices. In Tamir, T., editor, *Guided-Wave Optoelectronics*, pages 317–396. Springer-Verlag, Berlin, 2 edition.

Liu, A., Jones, R., Liao, L., Samara-Rubio, D., Rubin, D., Cohen, O., Nicolaescu, R., and Paniccia, M. (2004). A high-speed silicon optical modulator based on a metal semiconductor capacitor. *Nature*, 427:615–618.

Liu, M. M.-K. (1996). *Principles and Applications of Optical Communications*. McGraw-Hill, New York.

Mason, B., Ougazzaden, A., Lentz, C. W., Glogovsky, K. G., Reynolds, C. L., Przybylek, G. J., Leibenguth, R. E., Kercher, T. L., Boardman, J. W., Rader, M. T., Geary, J. M., Walters, F. S., Peticolas, L. J., Freund, J. M., Chu, S. N. G., Sirenko, A., Jurchenko, R. J., Hybertsen, M. S., Ketelsen, L. J. P., and Raybon, G. (2002). 40-Gb/s tandem electroabsorption

modulator. *IEEE Photon. Technol. Lett.*, 14(1):27–29.

Matsui, Y., Murai, H., Arahira, S., Kutsuzawa, S., and Ogawa, Y. (1997). 30-GHz bandwidth 1.55-μm strain-compensated InGaAlAs-InGaAsP MQW laser. *IEEE Photon. Technol. Lett.*, 9(1):25–27.

Miller, D. A. B., Weiner, J. S., and Chemla, D. S. (1986). Electric-field dependence of linear optical properties in quantum well structures: Waveguide electroabsorption and sum rules. *IEEE J. Quantum Electron.*, QE-22(9):1816–1830.

Miyazaki, Y., Tada, H., Tokizaki, S., Takagi, K., Aoyagi, T., and Mitsui, Y. (2003). Small-chirp 40-Gbps electroabsorption modulator with novel tensile-strained asymmetric quantum-well absorption layer. *IEEE J. Quantum Electron.*, 39(6):813–819.

Morton, P. A., Logan, R. A., Tanbun-Ek, T., Jr., P. F. S., Sergent, A. M., Montgomery, R. K., and Lee, B. T. (1992). 25 GHz bandwidth 1.55 μm GaInAsP p-doped strained multiquantum-well lasers. *Electron. Lett.*, 28(23):2156–2157.

Nagata, H. (2000). Activation energy of DC-drift of x-cut $LiNbO_3$ optical intensity modulators. *IEEE Photon. Technol. Lett.*, 12(4):386–388.

Nagata, H., Feke, G. D., Li, Y., and Bosenberg, W. (2004). DC drift of z-cut $LiNbO_3$ modulators. *IEEE Photon. Technol. Lett.*, 26(7):1655–1657.

Nakazawa, M., Kimura, Y., and Suzuki, K. (1989). Efficient Er^{3+}-doped optical fiber amplifier pumped by a 1.48 μm InGaAsP laser diode. *Appl. Phys. Lett.*, 54(4):295–297.

Noguchi, K., Mitomi, O., and Miyazawa, H. (1998). Millimeter-wave Ti:$LiNbO_3$ optical modulators. *J. Lightwave Technol.*, 16(4):615–619.

Noguchi, K., Mitomi, O., Miyazawa, H., and Seki, S. (1995). A broadband Ti:$LiNbO_3$ optical modulator with a ridge structure. *J. Lightwave Technol.*, 13(6):1164–1168.

Oh, M.-C., Zhang, H., Zhang, C., Erlig, H., Chang, Y., Tsap, B., Chang, D., Szep, A., Steier, W. H., Fetterman, H. R., and Dalton, L. R. (2001). Recent advances in electro-optic polymer modulators incorporating highly nonlinear chromophore. *IEEE J. Sel. Top. Quantum Electron.*, 7(5):826–835.

Okoshi, T. and Kikuchi, K. (1988). *Coherent Optical Fiber Communications*. KTK Scientific, Tokyo.

Olshansky, R., Hill, P., Lanzisera, V., and Powazinik, W. (1987). Frequency response of 1.3 μm InGaAsP high speed semiconductor lasers. *IEEE J. Quantum Electron.*, QE-23(9):1410–1418.

Petermann, K. (1991). *Laser Diode Modulation and Noise*. Kluwer Academic, Dordrecht, The Netherlands.

Pezeshki, B., Vail, E., Kubicky, J., Yoffe, G., Zou, S., Heanue, J., Epp, P., Rishton, S., Ton, D., Faraji, B., Emanuel, M., Hong, X., Sherback, M., Agrawal, V., Chipman, C., and Razazan, T. (2002). 20-mW widely tunable laser module using DFB array and MEMS selection. *IEEE Photon. Technol. Lett.*, 14(10):1457–1459.

Ralston, J. D., Weisser, S., Esquivias, I., Larkins, E. C., Rosenzweig, J., Tasker, P. J., and Fleissner, J. (1993). Control of differential gain, nonlinear gain and damping factor for high-speed application of GaAs-based MQW lasers. *IEEE J. Quantum Electron.*, 29(6):1648–1659.

Saleh, B. E. A. and Teich, M. C. (1991). *Fundamentals of Photonics*. Wiley-Interscience, New York.

Salgado, H. M., Ferreira, J. M., and OReilly, J. J. (1997). Extraction of semiconductor intrinsic laser parameters by intermodulation distortion analysis. *IEEE Photon. Technol. Lett.*, 9(10):1331–1333.

Sato, K. (2002). Semiconductor light sources for 40-Gb/s transmission systems. *J. Lightwave Technol.*, 20(12):2035–2045.

Sato, K., Kuwahara, S., Miyamoto, Y., and Shimizu, N. (2002). Direct modulation of a distributed feedback laser for 40-Gb/s very-short-reach optical links. In *Optical Fiber Commun. Conf.*, pages 416–417, Optical Society of America, Washington, D.C. Paper ThF2.

Schiess, M. and Carlden, H. (1994). Evaluation of the chirp parameter of a Mach-Zehnder intensity modulator. *Electron. Lett.*, 30(18):1524–1525.

Shi, Y., Wang, W., Bechtel, J. H., Chen, A., Garner, S., Kalluri, S., Steier, W. H., Chen, D., Fetterman, H. R., Dalton, L. R., and Yu, L. (1996). Fabrication and characterization of high-speed polyurethane-disperse red 19 integrated electrooptic modulators for analog system applications. *IEEE J. Sel. Top. Quantum Electron.*, 2(2):289–299.

Shi, Y., Zhang, C., Zhang, H., Bechtel, J. H., Dalton, L. R., Robinson, B. H., and Steier, W. H. (2000). Low (sub-1-Volt) halfwave voltage polymeric electro-optic modulator achieved controlling chromophore shape. *Science*, 288:119–122.

Suematsu, Y., Arai, S., and Kishino, K. (1983). Dynamic single-mode semiconductor lasers with a distributed reflector. *J. Lightwave Technol.*, LT-1(1):161–176.

Suematsu, Y., Iga, K., and Arai, S. (1992). Advanced semiconductor lasers. *Proc. IEEE*, 80(3):383–397.

Sugiyama, M., Doi, M., Taniguchi, S., Nakazawa, T., and Onaka, H. (2002). Driver-less 40 Gb/s $LiNbO_3$ modulator with sub-1 V drive voltage. In *Optical Fiber Commun. Conf.* Optical Society of America, Washington, D.C. postdeadline paper FB6.

Sun, C. K., Orazi, R. J., Pappert, S. A., and Burns, W. K. (1996). A photonic-link millimeter-wave mixer using cascaded optical modulators and harmonic carrier generations. *IEEE Photon. Technol. Lett.*, 8(9):1166–1168.

Tench, R. E., Delavaux, J.-M. P., Tzeng, L. D., Smith, R. W., Buhl, L. L., and Alferness, R. C. (1987). Performance evaluation of waveguide phase modulators for coherent systems at 1.3 and 1.5 μm. *J. Lightwave Technol.*, LT-5(4):492–501.

Tsuzuki, K., Yasaka, H., Ishibashi, T., Ito, T., Oku, S., Iga, R., Kondo, Y., and Tohmori, Y. (2004). 10-Gbit/s, 100-km SMF transmission using an InP-based n-i-n Mach-Zehnder modulator with a driving voltage of 1.0 V_{pp}. In *Optical Fiber*

Commun. Conf., osa. postdeadline paper PDP14.

Tucker, R. S. (1985). High-speed modulation of semiconductor lasers. *J. Lightwave Technol.*, LT-3(6):1180–1192.

Tucker, R. S. and Kaminow, I. (1984). High-frequency characteristics of directly modulated InGaAsP ridge waveguide and buried heterostructure lasers. *J. Lightwave Technol.*, LT-2(4):385–393.

Turner, E. H. (1966). High-frequency electro-optic coefficients of Lithium Niobate and Lithium Tantalate. *IEEE J. Quantum Electron.*, 2(4):128.

Walker, R. G. (1987). High-speed electrooptic modulation in GaAs/GaAlAs waveguide devices. *J. Lightwave Technol.*, LT-5(10):1444–1453.

Walker, R. G. (1991). High-speed III-V semiconductor intensity modulators. *IEEE J. Quantum Electron.*, 27(3):654–667.

Walklin, S. and Conradi, J. (1997). Effect of Mach-Zehnder modulator DC extinction ratio on residual chirp-induced dispersion in 10-Gb/s binary and AM-PSK duobinary lightwave systems. *IEEE Photon. Technol. Lett.*, 9(10):1400–1402.

Weisser, S., Larkins, E. C., Czotscher, K., Benz, W., Daleiden, J., Esquivias, I., Fleissner, J., Ralston, J. D., Romero, B., Sah, R. E., Schönfelder, A., and Rosenzweig, J. (1996). Damping-limited modulation bandwidths up to 40 GHz in undoped short-cavity $In_{0.35}Ga_{0.65}As$-GaAs multiple-quantum-well lasers. *IEEE Photon. Technol. Lett.*, 8(5):608–610.

Wen, Y. J., Nirmalathas, A., and Lee, D.-S. (2004). RZ/CSRZ-DPSK and chirped NRZ signal generation using a single-stage dual-electrode Mach-Zehnder modulator. *IEEE Photon. Technol. Lett.*, 16(11):2466–2468.

Wood, T. H. (1988). Multiple quantum well (MQW) waveguide modulators. *J. Lightwave Technol.*, 6(6):743–757.

Wooten, E. L., Kissa, K. M., Yi-Yan, A., Murphy, E. J., Lafaw, D. A., Hallemeier, P. F., Maack, D., Attanasio, D. V., Fritz, D. J., McBrien, G. J., and Bossi, D. E. (2000). A review of Lithium Niobate modulators for fiber-optic communications systems. *IEEE J. Sel. Top. Quantum Electron.*, 6(1):69–82.

Xu, C., Liu, X., and Wei, X. (2004). Differential phase-shift keying for high spectral efficiency optical transmissions. *IEEE J. Sel. Top. Quantum Electron.*, 10(2):281–293.

Yariv, A. (1997). *Optical Electronics in Modern Communications*. Oxford Univ. Press, Oxford, 5 edition.

Yu, J., Rolland, C., Somani, A., Bradshaw, S., and Yevick, D. (1996). Phase-engineered III-V MQW Mach-Zehnder modulator. *IEEE Photon. Technol. Lett.*, 8(8):1018–1020.